SAND2016-1286C

MECHANICAL SHOCK FAILURE PREDICTIONS OF A CANTILEVER STRUCTURE USING ENERGY RESPONSE SPECTRA METHODS

Carl Sisemore, Vit Babuška, Jason Booher
Sandia National Laboratories*
Albuquerque, NM 87185

ABSTRACT

Shock Response Spectra (SRS) are the standard for describing mechanical shock events and are used for design, analysis, and defining test specifications. The basic premise behind the SRS is that all time histories with the same SRS have the same shock damage potential. Energy response spectra have been used for some time as an alternate approach to describing mechanical shock events. This paper describes an analytical, numerical, and experimental study that compares traditional SRS with energy response spectra. A test structure supporting up to eight 3-D printed cantilever rods was designed for either shaker shock testing or drop table testing. Shock environments are developed such that the cantilever rods are predicted to fail during testing. Various options for tuning the frequency and failure stress of the test rods are incorporated to enable an adequate study of statistical parameters. The test results are compared to model predictions with a focus on using the test results to evaluate the failure prediction capabilities of the SRS and the energy response spectra for this simple problem.

INTRODUCTION

The shock response spectrum (SRS) is the standard method for defining mechanical shock events. The idea behind the SRS is that all time histories with the same SRS will have the same damage potential. The criticism of the SRS is that since it is a non-unique transform, there are theoretically an infinite number of time histories that can yield the same SRS. One alternative to the SRS is the energy spectrum. Energy spectra metrics for the analysis of shock data are nearly as old as the SRS. Hudson [1] and Housner [2] are generally credited with proposing the use of energy quantities to characterize transient base excitations resulting from earthquakes. Further analytical developments were published by Zahrah and Hall [3, 4] in the derivation of various energy terms. More recently Edwards presented a significant framework for the use of energy methods for shock analysis [5].

Recently, several programs at Sandia National Laboratories have adopted energy spectra as a straightforward metric to relate the severity of mechanical insults to structural capacity. The purpose of this metric is to gain insight into the system's capability, reliability, and to quantify the ultimate margin between the normal operating envelope and the likely system failure point—a system margin assessment. A true system margin assessment is only possible if some units are destructively tested. By performing destructive testing, a measure of the damage necessary to fail a component can be determined. This can then be related to the damage potential of a subsequent event on a new or used component and a measure of the remaining life in a component can be determined.

One of the fundamental concerns with the use of energy metrics is that the applicability domain and implementation details have not been completely defined for many problems of interest. Specifically, energy dissipation models are not well defined and energy dissipation is generally assumed to be a function of constant modal damping. The specific failure criteria are also not well defined since most failures are localized failures as opposed to global failures. Most programs are concerned with functional failures of their equipment which may not necessarily be related to a gross structural failure. Many times a functional failure can be induced by tripping a circuit breaker or cracking a solder joint while the structure remains completely intact.

The purpose of this investigation was to build a series of simple structures, test them to failure, and compare the failures seen with various damage metrics based on SRS and energy spectra. The goal of this study was to examine

* Sandia National Laboratories is a multi-program laboratory managed and operated by Sandia Corporation, a wholly owned subsidiary of Lockheed Martin Corporation, for the U.S. Department of Energy's National Nuclear Security Administration under contract DE-AC04-94AL85000.

both first passage failures and low-cycle fatigue failures. One of the fundamental benefits often espoused about the energy metrics are their ability to consider cumulative damage from multiple insults [5]. Therefore, a simple study of repetitive shock to failure, or low cycle fatigue, seemed very appropriate to this research.

The structure selected for this study was a cantilever beam. A cantilever beam was selected due to its relative simplicity and ease of manufacture, but also because it is representative of many simple real-world components of interest.

The long term goal for this multi-year project is to develop the experimental and mathematical framework such that transient shock data from the field can be collected and analyzed from a real-world system level test. These data would be used to generate a test specification for subsequent component testing in the laboratory. The method used to generate the test specification could be based on an absolute acceleration SRS, and pseudo-velocity SRS, or an energy spectrum. This test specification can then be tested in the laboratory and the resulting laboratory generated failures compared to the system level field test failures to determine the best metric for evaluating potential component failures and also quantify the remaining margin to failure for nondestructive tests and shock events.

ENERGY SPECTRUM OVERVIEW AND EQUATIONS

The concept of energy spectrum is based on the law of conservation of energy. Conservation of energy requires that all of the energy input to a system must be absorbed, dissipated, or converted to kinetic energy. Shock loading transmits energy to a system in a very short time which may then alter or damage the system. The relationship for energy imparted to a system was presented by Zahrah and Hall in their derivation of earthquake energy relations [4].

$$E_I^* = \int_0^z M\ddot{z}(t)dz + \int_0^Z C\dot{z}(t)dz + \int_0^z R^* z(t)dz. \tag{1}$$

In the Equation (1), M is the system mass, C is the damping coefficient, $z(t)$ is the relative displacement of the system with respect to ground, and R^* is the system restoring force. The input energy E_I^* in the above equation is given in terms of the base or ground acceleration $\ddot{x}$ by the integral:

$$E_I^* = -\int_0^z M\ddot{x}(t)dz = -M\int_0^z \ddot{x}(t)dz. \tag{2}$$

Since the integral relations in Equations (1) and (2) can be calculated independently of the system mass, the equations can be redefined in terms of energy per unit mass. Thus, the expressions become:

$$E_I = \frac{E_I^*}{M} = -\int_0^z \ddot{x}(t)dz \tag{3}$$

$$E_I = \int_0^z \ddot{z}(t)dz + 2\zeta\omega\int_0^z \dot{z}(t)dz + \int_0^z Rz(t)dz. \tag{4}$$

In Equation (4), Zahrah and Hall, replaced the system restoring force term R^* with the mass normalized value R by which they defined $Rz(t)$ to represent the resistance per unit mass of the system or structure, which is equal to $\omega^2 z(t)$. Thus, it is apparent that Zahrah and Hall used the variable R^* to represent the system stiffness which is more commonly denoted k in the mechanical engineering literature and $R = k/m$.

To simplify the numerical integration, the integrals in Equations (3) and (4) are converted to time domain integrals by the relationship $dz = \dot{z}dt$. This is advantageous since the data are traditionally collected as acceleration time histories. Thus, after performing the change of variables, substituting for R, and equating Equations (3) and (4), the energy expression becomes:

$$-\int_0^t \ddot{x}(t)\dot{z}(t)dt = \int_0^t \ddot{z}(t)\dot{z}(t)dt + 2\zeta\omega\int_0^t \dot{z}(t)^2 dt + \omega^2\int_0^t z(t)\dot{z}(t)dt. \quad (5)$$

The first term on the right hand side of Equation (5) represents the kinetic energy, E_K, of the system. The second term represents the energy dissipated by damping, E_D. The third term represents the sum of the hysteretic energy, E_H, plus the strain energy, E_S. The previous integral expressions can be shown to be identical to the matrix notation energy balance expressions presented by Edwards [5].

The two most common energy spectra metrics currently selected for use in a system margin assessment are the absorbed energy and dissipated energy spectra as defined by the previous equations. However, any of the four energy spectrum terms could be used for a margin assessment if the domain of applicability were well understood. In theory, it is also possible to use any of the above energy metrics as a measure of relative severity between two events.

TEST FIXTURE DESIGN DETAILS

Before any data were collected to evaluate spectral results, an adequate test fixture and test article had to be developed. Some of the primary design and performance goals for the test fixture were:

- Ability to test multiple cantilever beams simultaneously.
- Ability to control the cantilever beam failure location and tailor the dynamic response.
- Sufficient rigidity to not unduly influence the dynamic response of the cantilever beams.

Several design iterations for the test fixture were performed and finite element analysis was used to verify structural and dynamic performance of the test fixture. The final design consisted of an aluminum base plate with a solid vertical tower capable of supporting up to eight cantilever beams simultaneously. A photograph of the final text fixture design is shown in Figure 1 with eight cantilever beams installed.

In addition to the test fixture, several iterations for the design of the cantilever test structures were also performed. Finite element analysis was used to get an initial estimate of the fundamental natural frequency for the various beams to be tested. Some of the primary design and performance goals for the cantilever test articles were:

- Easy and economical to manufacture.
- Ability to include a stress concentration in the cantilever beam to control the failure mode.
- Ability to tailor the fundamental resonant frequency of the beam.

The cantilever beams used for this investigation were made of ABS plastic using 3D printing by the Sandia National Laboratories Additive Manufacturing group. These beams were easily made, relatively inexpensive, and a stress concentration notch was easily added during manufacturing. A photograph of the six different cantilever beam configurations used for this study is shown in Figure 2. Clamp-on aluminum and steel collars were added to the free ends of the beams to tailor the natural frequency and increase the beam stress under shock. A set of the aluminum collars can be seen in Figure 1. Most tests made use of a single steel collar positioned at the free end. A few tests used the aluminum collars and other tests used two collars to create higher stresses in the beam.

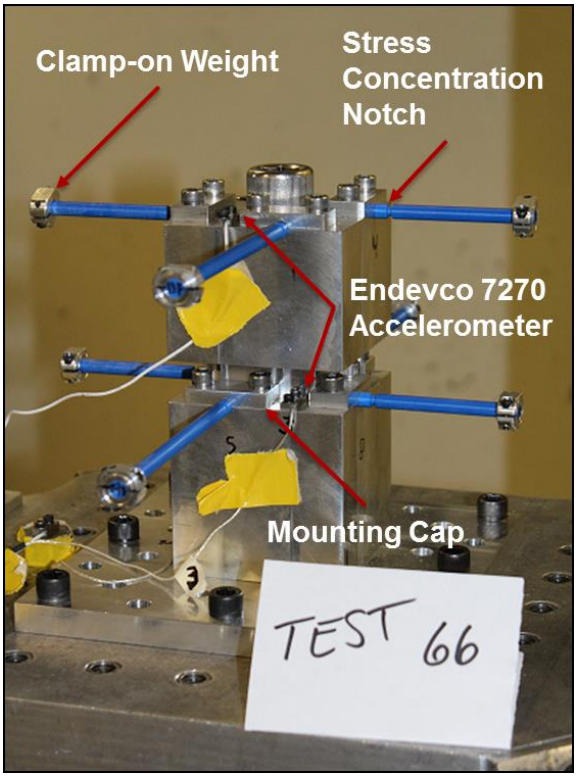

Figure 1. Photograph of the Text Fixture with 3D Printed Cantilever Beams Installed and Ready for Testing

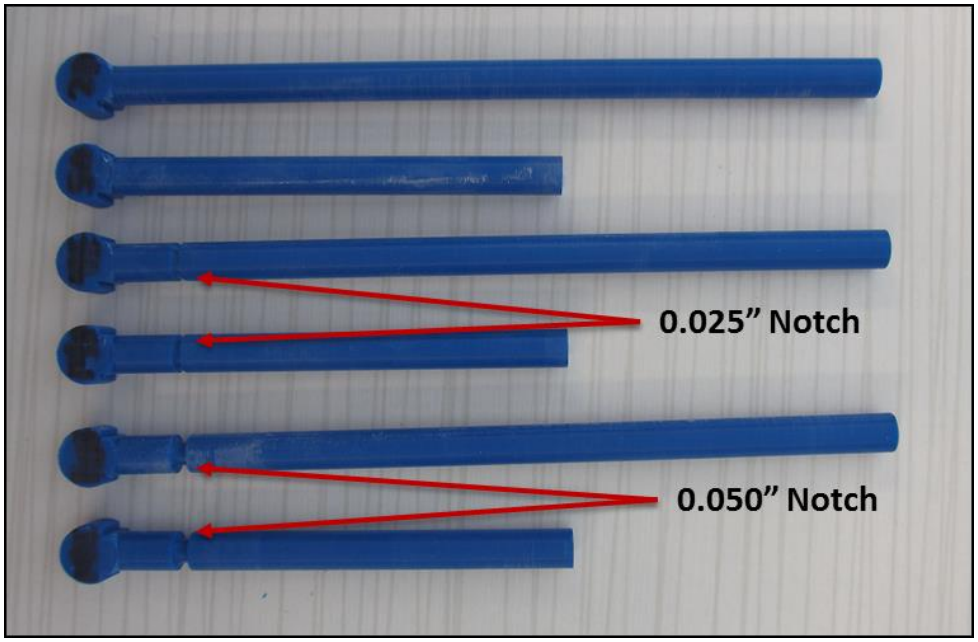

Figure 2. Photograph of Cantilever Beams Used for Testing

Finally, a finite element analysis of the test fixture was performed with the test articles installed to ensure that the dynamics of the two systems were sufficiently separated so that the test results would not be corrupted by test fixture responses. As expected, the fundamental vertical and lateral frequencies of the test fixture's upright tower are significantly removed from the beam frequency so that dynamic coupling was not seen during the tests.

ELASTIC PROPERTIES OF 3D PRINTED BEAMS

In order to make reasonable predictions of test failures, it is necessary to understand the material properties of the items being tested. A series of static pull tests was performed on various 3D printed tensile coupons prior to having the full lot of test specimen printed. During this phase of the study, it was discovered that the 3D printer had several properties that significantly affected the strength and performance of the resulting beams. Specifically, the size of the print head and the raster orientation for the beams were the dominant parameters. Tensile coupons were manufactured using both a 5mil print head and a 10mil print head and coupons were made with the raster orientation lengthwise (coupon printed horizontally on the bed) and crosswise (coupon printed vertically on the bed) to the coupon. The results from the various tensile tests are presented in Figure 3. The inset photograph in Figure 3 shows a micrograph of the fracture surface from one of the crosswise raster tensile specimen. Clearly the failure occurred between print layers and the raster pattern is readily discernable.

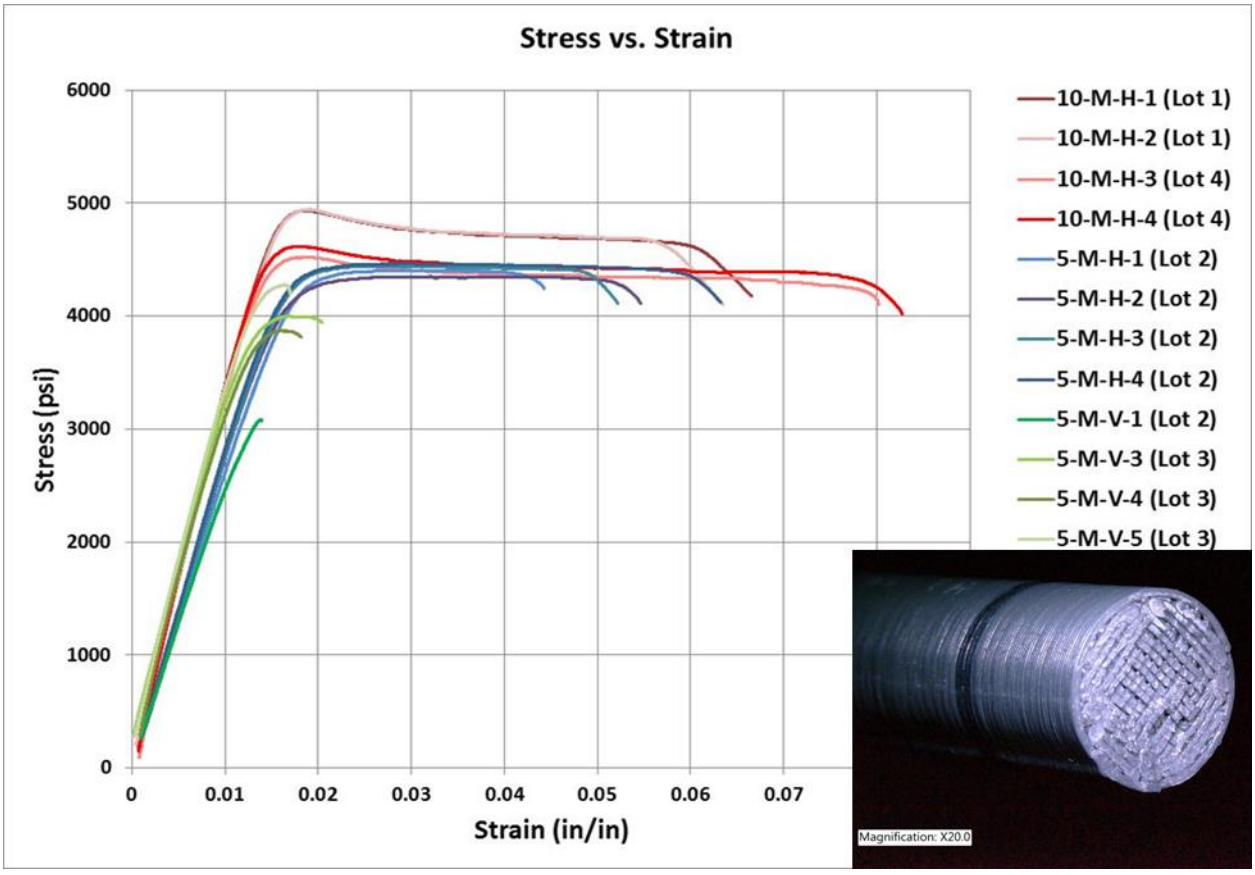

Figure 3. Stress-Strain Data from Tensile Specimen and Inset Picture Showing Fracture Surface for Specimen with Crosswise Raster

The results indicated that tensile coupons printed in the vertical orientation using a crosswise raster exhibited a brittle failure whereas the coupons printed horizontally on the print bed using a lengthwise raster exhibited a ductile type of failure. The vertically printed specimen also showed more variability in the failure strain than the horizontally printed specimen. It was also noted that the 5mil print head seemed to have slightly lower strain to failure than the 10mil print head.

All of the cantilever beams used for the shock tests were manufactured using a 5mil print head with a crosswise raster. This was intentionally done to produce clear pass-fail results in the cantilever beams tested since brittle failures are typically sudden and total.

SHOCK TESTING OVERVIEW

A total of 72 3D printed cantilever beams were tested on a drop table. The tests were conducted using nine sets of eight beams per test (four 5 inch beams and four 3 inch beams per test) on a drop table. Initial tests were performed by incrementally stepping up the input shock load until all eight beams failed. Typically most beams failed after just a few shock events. The second round of testing attempted to quantify low-cycle fatigue failures for cantilever beams of the same design. For the low-cycle fatigue tests, a test level less than the failure level was selected and that test was repeated until all beams failed. Figure 4 shows a time history plot from the four accelerometers mounted on the carriage and test fixture during test 70. This profile was typical of the acceleration results seen throughout the testing. Figure 5 shows the acceleration SRS for the carriage mounted accelerometer from the same test, Test 70.

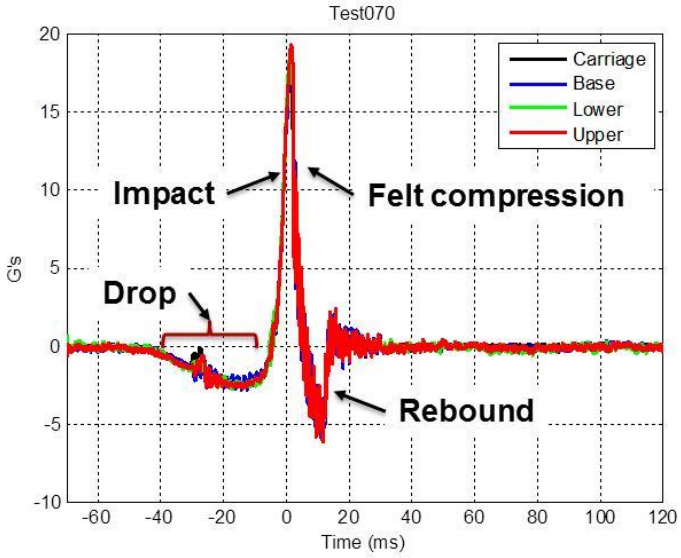

Figure 4. Typical Acceleration Profile from Drop Table Tests

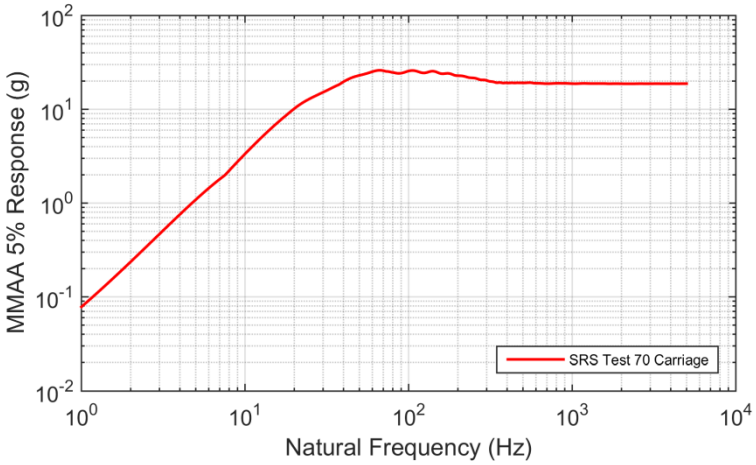

Figure 5. Typical Acceleration SRS Profile at the Drop Table Carriage

Approximately 148 shock tests were performed on the drop table. Of these tests, all failures were brittle failures as expected, although some of the beams did not fail completely in a single shock. Some beams cracked and sagged downward and detached on the subsequent shock. For these beams, failure was considered to have occurred on the first shock that resulted in a visible crack and deformation. Figure 6 shows an interesting photograph taken after

Test 70 which shows all three types of failures seen during testing. The beam in the front lower clamp is completely broken free and bounced clear of the table. The beam on the lower right side of the upright is clearly cracked and sagging. The beam on the lower left is severely cracked and apparently hanging by a "thread" of plastic.

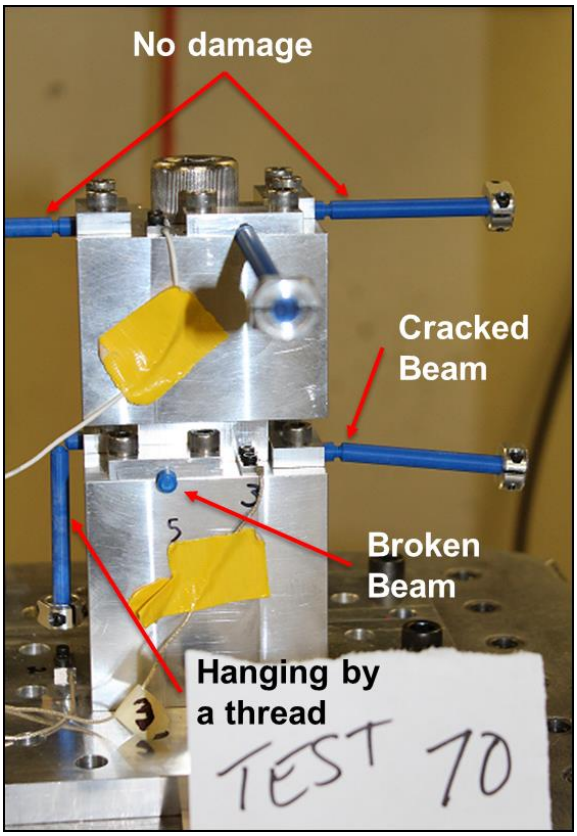

Figure 6. Summary of Typical Cantilever Beam Failures Types Seen During Shock Testing

SHOCK TESTING RESULTS

The first tests were conducted to determine the failure points of all beam configurations and to compare the finite element beam model predictions to the actual results. Since drop table testing is a series of distinct events with definite increments to the shock load, it is not possible to determine the exact failure point. The cantilever beam specimen would be intact after one shock and fail during the next shock. The exact failure point is then known to be between the last two shocks, but since the tests were conducted in increments, and the beams were broken, no further refinement was possible. All of the drop tests in this portion of the experiments were designed to achieve a nominal 90 Hz haversine pulse. This frequency was selected to ensure that all the beams tested had natural frequencies well below the primary shock pulse frequency. One problem encountered during testing was that the drop table had a minimum shock level. The table available for testing was unable to hit with less than about 20g peak acceleration.

Table 1 summarizes the results from the first passage shock tests. For this test series the finite element predictions and the observed test failures agreed very well for all beams except for the 5 inch un-notched beams. Two explanations are possible for the over-prediction of the 5 inch un-notched beams. First, the failure location was not completely predictable for the un-notched beams. Most beams failed close to the test fixture upright but variations up to approximately 0.25 inches were seen. Second, the number of shocks required to induce failure may have started to resemble low cycle fatigue testing for some of the more robust specimen. This would have also lowered the failure levels over the predicted failure points.

Table 1. First Passage Tests Beam Failure Summary

Beam Length	Notch Depth	Observed Test Failure	Predicted Failure
5 in	None	32.0g → 62.5g	64.5g
5 in	0.025 in	30.5g → 41.5g	38.5g
5 in	0.050 in	< 27g	18.8g
3 in	None	42.5g → 98.0g	58.8g
3 in	0.025 in	30.5g → 41.5g	37.4g
3 in	0.050 in	< 27g	20.4g

Figure 7 shows a plot of the absorbed energy spectrum calculated from the first passage failure tests of the 5 inch beams with the 0.025 inch notch. For this test series, four beams were tested and all four beams failed on the third drop test. The three shock levels are shown in the figure: 26g, 31.5g and 41.5g which indicates that the onset of failure should be located between 31.5g and 41.5g. Ideally it would have been advantageous to uses smaller increments between tests; however, the resolution of the drop table was somewhat limited at these low levels. The failure predictions were obtained from the finite element model using a maximum strain failure criteria based on the average failure strain measured in the tensile specimen tests. The failure predictions were very good in this example with the predicted absorbed energy at failure faring through the absorbed energy spectrum from the final drop test. The vertical dashed line in Figure 7 represents the cantilever beam first resonant frequency which is the frequency line that is assumed to be predominately responsible for the beam failure, and at this frequency the absorbed energy spectra exceeds the failure prediction.

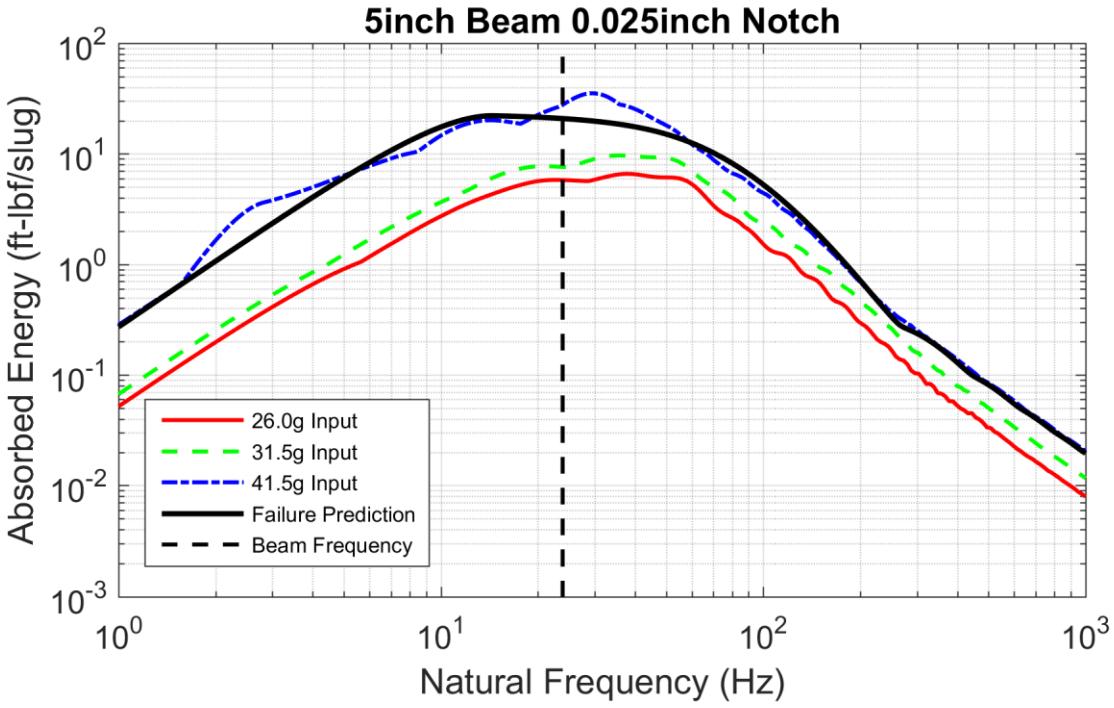

Figure 7. 5 inch 0.025 inch Notch First Passage Failure Testing Energy Spectrum Results Compared to Failure Prediction

Figure 8 shows a similar plot of the absorbed energy spectrum versus the predicted absorbed energy spectrum for the 3 inch long cantilever beams with the 0.025 inch notch. As before, this test series tested four beams and all four beams failed on the third drop test. Three shock levels are shown in the figure: 21.5g, 30.5g, and 40.5g which indicate that the onset of failure is between 30.5g and 40.5g. Once again, the predicted failure was obtained from the finite element model using the peak strain failure criteria. The absorbed energy spectrum at failure again passes

through the calculated absorbed energy spectrum from the last drop test. Here again, the vertical dashed line in Figure 8 represents the first resonant mode of the cantilever beam that is assumed to be predominately responsible for the failure, and at this frequency the absorbed energy spectra exceeds the failure prediction.

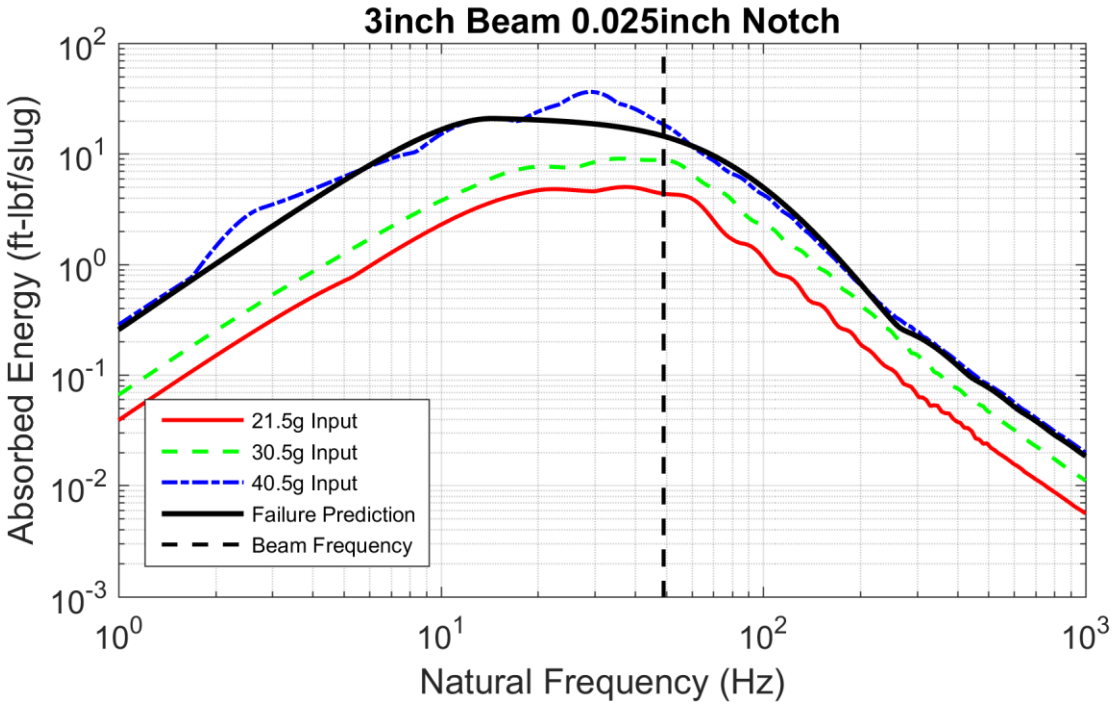

Figure 8. 3 inch 0.025 inch Notch First Passage Failure Testing Energy Spectrum Results Compared to Failure Predictions

One of the primary benefits of energy methods is their applicability to multiple shock scenarios. In fact, this is an often touted advantage over traditional SRS techniques [5]. It is well known that the SRS of a time signal containing two identical shocks is the same as the SRS for one of the two shocks provided the two shocks occur sufficiently separated in time for the response to complete decay to zero. Since the SRS is a maximum response, it will not change or increase as multiple identical shock events are added to the time history. Energy spectrum techniques, in contrast, integrate over the entire time signal, adding the energy contained under the time history curve. As a result, certain energy spectrum from a signal containing two identical shocks will be twice as large as those from a single shock.

To test this theory, the second phase of testing tried to study the effects of low-cycle fatigue on the 3D printed plastic cantilever beams. To perform this testing the drop parameters from the drop table shock immediately prior to beam failure from the first passage failure tests were used and the shocks were repeated at nominally the same level until all of the beams in the set failed. For example, the 5 inch 0.025 inch notched beams were tested at a nominal shock level of 31.7g, corresponding to the second shock in Figure 7, which was the shock prior to the one that failed the beam. This shock was repeated 27 times until all of the beams failed. Some minor variability between shock events was seen due to the nature of the low levels being used on the drop table. This variability was not significant, although each shock time history was recorded and used throughout the calculations and results presented here.

Table 2 summarizes the results of the low-cycle fatigue tests conducted on the various cantilever beams. For each beam type tested, the range of number of shocks to fail is provided as well as the average. All of the low-cycle fatigue tests were conducted with four identical beams except for 5 inch 0.050 inch beams where only three beams were available for testing. The ranges of shocks to fail the beams were generally quite wide and indicative of the large variability typically seen in typical S-N type fatigue data.

Table 2. Low-Cycle Fatigue Test Beam Failure Summary

Beam Length	Notch Depth	Tip Weight	Tested Shock Level	% of Strain Allowable	Average Hits to Fail	Range of Hits to Fail
5 in	None	0.028 lbf	44.8g	61%	36	27 → 47
5 in	0.025 in	0.028 lbf	31.7g	77%	19	14 → 27
5 in	0.050 in	0.010 lbf	22.0g	61%	5	2 → 10
3 in	None	0.057 lbf	38.8g	53%	3	1 → 6
3 in	0.025 in	0.028 lbf	31.5g	78%	12	1 → 18
3 in	0.050 in	0.010 lbf	21.7g	44%	13	4 → 33

Figure 9 and Figure 10 show plots summarizing the low-cycle fatigue test results from the 5 inch 0.025 inch beam tests. The finite element failure prediction is identical to the failure prediction shown previously in the first passage failure plots and is based on the simple single strain to failure model. The absorbed energy spectra, shown in Figure 9, for the first shock shows that the energy was below the single shock absorbed energy spectrum at failure at all natural frequencies. This shock was repeated until all of the beams failed. In this test, the four beams failed after 14, 25, 20, and 27 shocks with an average of 19 shocks to failure. Figure 9 also shows the sum of the absorbed energy spectra for all of the subsequent shocks leading up to beam failure. As can be seen, all of the failures occurred well beyond the first passage failure predictions. A similar plot of the input energy spectrum is shown in Figure 10. It was shown previously that the first passage failure predictions were really quite accurate for increasing amplitude shocks, but neither the absorbed energy spectrum nor the input energy spectrum comparison for repetitive lower level shocks appear to agree well with the test results. It is apparent from the test results, that the beams can absorb more energy from multiple low level shocks than from a single high level shock.

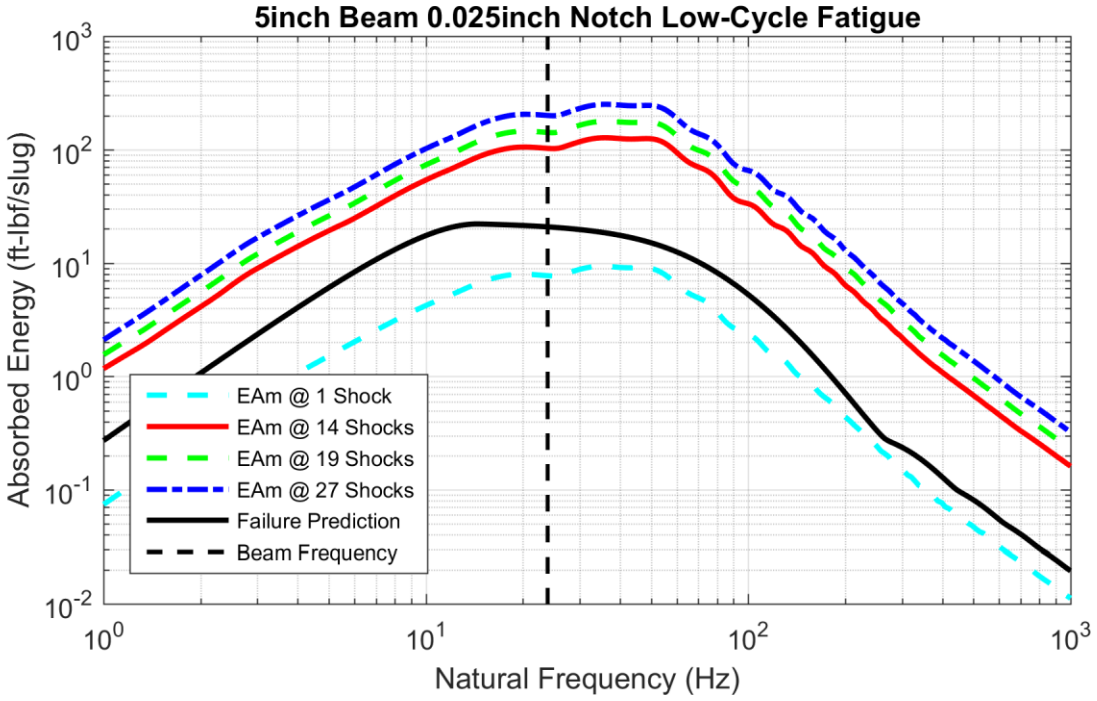

Figure 9. 5 inch 0.25 inch Notch Low-Cycle Fatigue Failure Testing Absorbed Energy Spectrum Results Compared to First Passage Failure Prediction

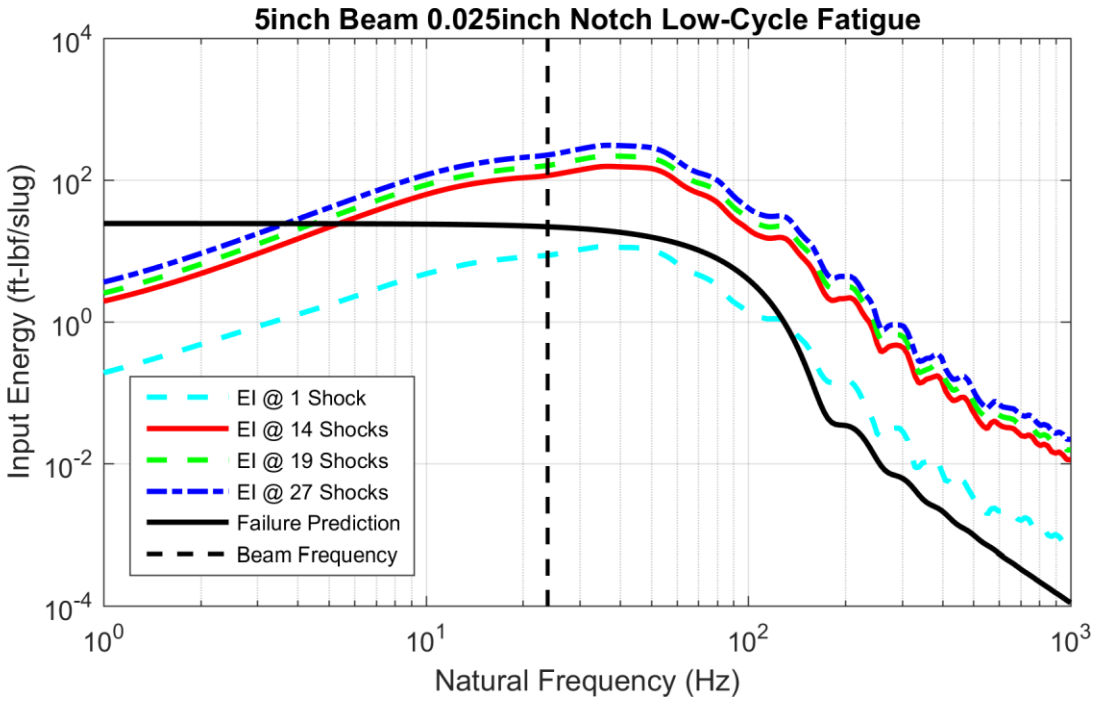

Figure 10. 5 inch 0.25 inch Notch Low-Cycle Fatigue Failure Testing Input Energy Spectrum Results Compared to First Passage Failure Prediction

Figure 11 and Figure 12 show similar plots comparing the absorbed energy spectrum and input energy spectrum from the low-cycle fatigue tests for the 3 inch 0.025 inch beams. For these tests, the failure results were more disparate than those shown in Figure 9 for the 5 inch beams. One of the 3 inch beams failed on the first shock at a level below the finite element failure prediction and less than the failures seen in the first passage tests. It is possible that there was an undetected flaw in the specimen but it is equally possible that the result represents expected variation since relatively few samples were used for testing. The 3 inch 0.025 inch notch samples failed at 1, 12, 18 shocks (two beams failed on the last shock) with an average of 12 shocks to failure. Here again, the comparison of the summation of the absorbed energy spectrum and the input energy spectrum over all the shocks indicates that all but the first failure occurred well beyond the first passage failure prediction. In general it can be concluded that a chain of lower level shocks is not as damaging as a single higher level shock, although the failure of one beam with the first hit is clearly indicative that testing was performed near the failure point and component variability can play a significant role.

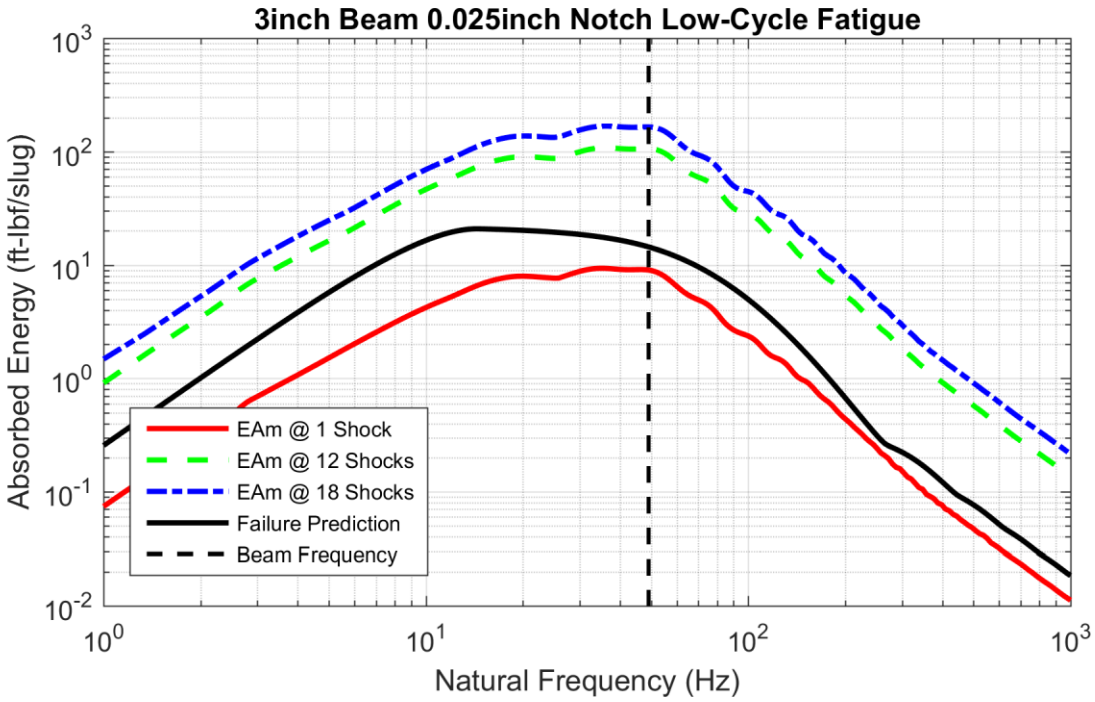

Figure 11. 3 inch 0.025 inch Notch Low-Cycle Fatigue Failure Testing Absorbed Energy Spectrum Results Compared to First Passage Failure Prediction

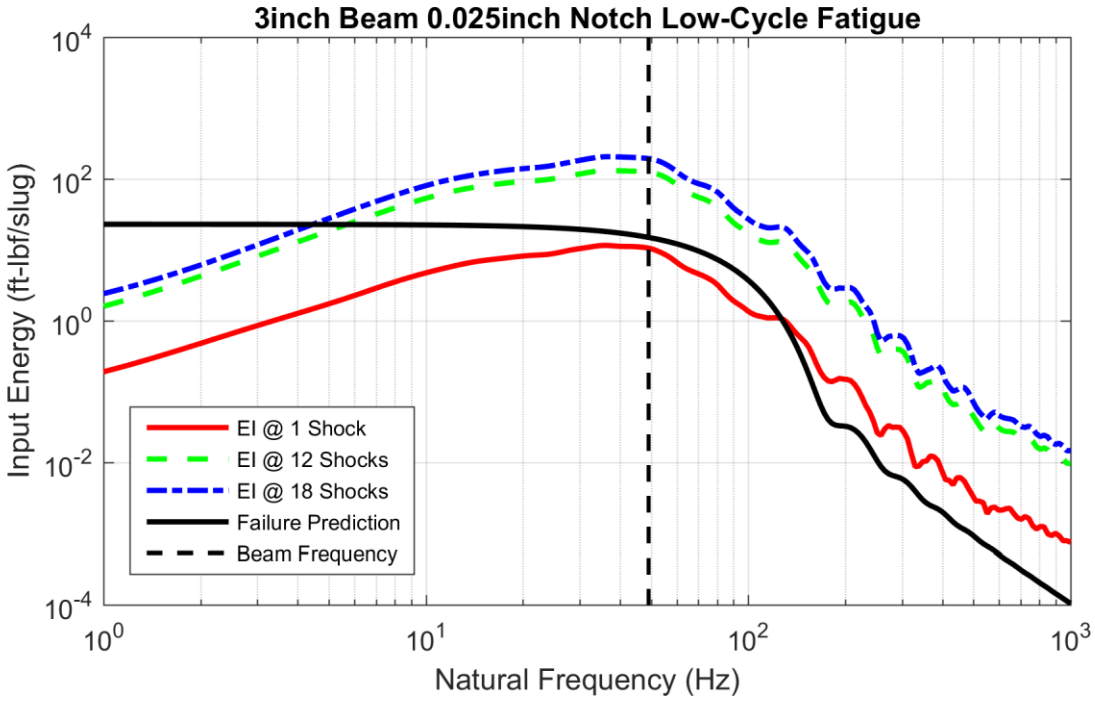

Figure 12. 3 inch 0.025 inch Notch Low-Cycle Fatigue Failure Testing Input Energy Spectrum Results Compared to First Passage Failure Prediction

CONCLUSIONS

This paper presents the results of a series of tests on cantilever beams comparing failure predictions using absorbed energy spectra for both first passage failure tests and low-cycle shock fatigue tests. The 3D printed ABS cantilever beams used for this testing proved to be remarkably consistent throughout a manufacturing lot. Reasonable agreement was seen even in lot to lot comparisons. One important lesson learned is that tensile coupons should be printed with each lot in order to measure the exact properties for that lot.

Energy spectrum techniques proved to be a reasonable predictor of single shock failure levels when compared to the absorbed energy spectrum of a calculated haversine shock based on beam failure strain. The relationship of failure from accumulated shocks, low-cycle fatigue, to single shock failure using the absorbed energy spectrum does not appear to be linear and needs considerable further research. In all cases, the cantilever beams used here were able to withstand a longer series of shocks at a level below the single shock failure level than would be expected by a summation of absorbed energy.

REFERENCES

1. Hudson, D. E., "Response Spectrum Techniques in Engineering Seismology," *Proceedings of the World Conference on Earthquake Engineering*, Berkeley, California, 1956, pp. 4.1–4.12.
2. Housner, G. W., "Behavior of Structures During Earthquake," *Journal of the Engineering Mechanics Division (ACSE)*, 1959, Vol. 85, No. 4, pp. 109–129.
3. Zahrah, T. F. and Hall, W. J., "Earthquake Energy Absorption in SDOF Structures," *Journal of Structural Engineering*, Vol. 110, No. 8, August 1984, pp. 1757–1772.
4. Zahrah, T. F. and Hall, W. J., "Seismic Energy Absorption in Simple Structures," *Civil Engineering Studies, Structural Research Series No. 501*, University of Illinois, Urbana, Illinois, July 1982.
5. Edwards, T. S., *Using Work and Energy to Characterize Mechanical Shock*, Technical Report SAND2007–0851J, Sandia National Laboratories, Albuquerque, New Mexico, February 2007.